

# Measuring the wavenumber of guided modes in waveguides with linearly varying thickness

Ludovic Moreau, Jean-Gabriel Minonzio, Maryline Talmant, Pascal Laugier

#### ▶ To cite this version:

Ludovic Moreau, Jean-Gabriel Minonzio, Maryline Talmant, Pascal Laugier. Measuring the wavenumber of guided modes in waveguides with linearly varying thickness. Journal of the Acoustical Society of America, 2014, 135 (5), pp.2614-2624. 10.1121/1.4869691. hal-01394317

## HAL Id: hal-01394317 https://hal.sorbonne-universite.fr/hal-01394317

Submitted on 9 Nov 2016

**HAL** is a multi-disciplinary open access archive for the deposit and dissemination of scientific research documents, whether they are published or not. The documents may come from teaching and research institutions in France or abroad, or from public or private research centers.

L'archive ouverte pluridisciplinaire **HAL**, est destinée au dépôt et à la diffusion de documents scientifiques de niveau recherche, publiés ou non, émanant des établissements d'enseignement et de recherche français ou étrangers, des laboratoires publics ou privés.

## Measuring the wavenumber of guided modes in waveguides with

# linearly varying thickness 2 3 4 Ludovic Moreau, a) Jean-Gabriel Minonzio, A) Maryline Talmant, a) and Pascal Laugier a) 5 6 UPMC University Paris 06, Unité Mixte de Recherche 7623, LIP, F-75005, Paris, 7 8 9 Running title: guided modes in a thickness-varying waveguide 10 11 December 17<sup>th</sup> 2013 12 Revision February 20<sup>th</sup> 2014 13 14

\_

1

<sup>&</sup>lt;sup>a)</sup> Also at : CNRS, Unité Mixte de Recherche 7623, Laboratoire d'Imagerie Paramétrique, 15 rue de l'école de médecine F-75006, Paris, France.

#### **Abstract**

Measuring guided waves in cortical bone arouses a growing interest to assess skeletal status. In most studies, a model of waveguide is proposed to assist in the interpretation of the dispersion curves. In all the reported investigations, the bone is mimicked as a waveguide with a constant thickness, which only approximates the irregular geometry of cortical bone. In this study, guided mode propagation in cortical bone-mimicking wedged plates is investigated with the aim to document the influence on measured dispersion curves of a waveguide of varying thickness and to propose a method to overcome the measurement limitations induced by such thickness variations. The singular value decomposition-based signal processing method, previously introduced for the detection of guided modes in plates of constant thickness, is adapted to the case of waveguides of slowly linearly variable thickness. The modification consists in the compensation at each frequency of the wavenumber variations induced by the local variation in thickness. The modified method, tested on bone-mimicking wedged plates, allows an enhanced and more accurate detection of the wavenumbers. Moreover, the propagation in the directions of increasing and decreasing thickness along the waveguide is investigated.

PACS numbers 43.35 Cg, 43.80.Vj, 43.20.Ye, 43.20.Mv, 43.60.Fg, 87.15.La

## I. Introduction

The cortical envelope of long bones has been reported to behave like a waveguide with respect to ultrasound propagation.<sup>1, 2</sup> The potential of guided waves as a diagnostic tool to assess bone status is now considered by several research groups mostly because the propagation characteristics of guided waves convey information on bone strength-relevant characteristics, such as cortical thickness and elasticity, that cannot be readily assessed by currently available X-ray imaging modalities.<sup>3, 4</sup> Moreover, compared to X-rays, ultrasound technology is also less expensive, non-ionizing and portable.

Guided mode propagation in cortical bone is investigated using the so-called axial transmission technique in which the signal propagating along the bone axis is recorded at multiple positions aligned along a same side of a skeletal site, by moving a receiver, <sup>5-8</sup> or moving both the transmitter and the receiver in parallel, <sup>9</sup> or using a multiple element array, <sup>10-12</sup>, or using photo-acoustic excitation and optical detection. <sup>13</sup> The first version of the axial transmission approach consisted in recording the time-of-flight of the earliest component of the signal recorded at the receivers, the so-called first arriving signal (FAS). <sup>14-18</sup> In subsequent developments, a multiple frequency approach in which FAS velocity is measured at different frequencies has also been described. <sup>9, 19, 20</sup>

A different approach, based on a more complete analysis of the recorded time signals, consists in detecting one or more particular guided modes which are then identified by coupling the experimental analysis to a model of the waveguide. For example, Moilanen *et al.* have proposed to specifically detect a thickness-sensitive fundamental flexural guided wave.<sup>12, 21</sup> Other authors analyze the full response of the waveguide using various signal processing techniques (*e.g.*, time-frequency distributions, two-dimensional spatio-temporal Fourier transform) to measure the dispersion curves of multiple guided modes.<sup>6, 22</sup>

A method combining an ultrasonic multi-element array with a singular value

decomposition (SVD)-based signal processing has recently been proposed by our group to measure the propagation of guided waves in cortical bone.<sup>11, 23</sup> A small array has been specifically designed for *in vivo* measurements and to accommodate to the limited access to cortical skeletal sites, such as the distal radius at the forearm. The method, extensively described in previous publications, has been tested successfully with bone mimicking plate-like waveguides<sup>11, 23-25</sup> and *ex vivo* human radius specimens.<sup>26, 27</sup>

In most studies, a model of waveguide is proposed to assist in the interpretation of the dispersion curves. Various models have been proposed,<sup>2</sup> including the free 2-D elastic plate,<sup>11, 23, 28</sup> the free 2-D gradient elastic plate<sup>29, 30</sup> or the free 3-D elastic tube.<sup>6, 13, 27, 31</sup> They only approximate the complex heterogeneous and geometrically irregular structure of cortical bone. In particular, in all the reported investigations, the bone is mimicked as a waveguide with a constant thickness. However, experimental observations indicate that at the distal radius, the most frequently investigated skeletal site using axial transmission, the thickness of the cortical shell varies slowly, being thinner at the proximal end (epiphysis) and thicker in the mid section (diaphysis). To the authors' best knowledge, the effect of a varying bone cortical thickness on guided modes dispersion curves has not been reported so far.

Propagation in waveguide with variable thickness has been studied theoretically, <sup>32-34</sup> experimentally <sup>35-37</sup> or numerically <sup>36, 38</sup> in the context of non destructive testing, <sup>39</sup> ocean waveguide, <sup>40</sup> or study of musical instruments such as horns. <sup>34</sup> In the context of ultrasonic characterization of bone, the aim of this paper is first to document the influence on measured dispersion curves of a waveguide of varying thickness and second to propose a method to overcome the measurement limitations induced by such thickness variations. A free 2-D elastic plate waveguide *with slowly linearly varying thickness* (typical to the configuration encountered at the distal human radius), supporting "adiabatic" propagating waves, is considered. The main advantage of such a model rather than a more realistic cortical bone

geometry or a not-rigorously linear variation in thickness is its simplicity: it allows deriving simple analytic expressions to describe the impact on the wave numbers of a varying thickness and facilitates understanding of the effect of the varying thickness on guided mode propagation. The disadvantage, of course, is that it only approximates complex bone structure. However, 2-D elastic plate or tube models with constant thickness have previously demonstrated a high level of consistency with experimental observations in cortical bone measured *ex-vivo*.

The aims of this paper are twofold, (1) to gain insights into the influence of a slowly linearly varying thickness of the waveguide on guided modes, (2) to propose a method, adapted from the currently existing SVD-based signal processing, to overcome the guided mode measurement limitations induced by these thickness variations. The paper is organized as follows. A model is proposed to predict the effect on guided mode wavenumbers of a waveguide of slowly linearly varying thickness (Sec. II). The predicted variations are taken into account in the adapted signal processing technique (Sect. III). Both the model and the adapted signal processing are then validated on experimental data from bone-mimicking wedged plates (Sec. IV). Finally, the direction of propagation of the guided waves is investigated.

## II. Influence of the varying thickness on adiabatic mode wavenumbers

#### A. Cortical bone is considered as a plate with a linear varying thickness

In order to illustrate the thickness variation of the cortical bone, two cross-sections images derived from 3-D X-ray computed tomography data (Siemens, Somaton 4 Plus, 200 µm-voxel size) of a human distal radius are shown in Fig. 1(a). These images, excerpted from Ref. 41, are illustrative of the general structure of the cortical shell of the 39 human radius specimens for which the FAS velocity was reported in Ref. 16. As illustrated on the

longitudinal cross-section, the cortical thickness decreases regularly with a moderate slope from the mid-diaphysis (left) to the epiphysis (distal end, right). By reanalyzing the X-ray computed tomography radius database, the thickness variation along the bone axis in the measurement region, highlighted with a white square on Fig. 1(a), can reasonably be approximated with a linear fit. The analysis of the 39 excised human radii evidenced a mean cortical thickness of  $2.2 \pm 0.6$  mm with a mean cortical angle equal to  $1.2 \pm 0.7^{\circ}$ .

The relevance of a plate versus a tube model to represent the cortical shell of human radius specimens has been discussed in several studies.<sup>6, 27, 31</sup> Predictions using a plate model have been found to fit well the experimental data observe on *ex vivo* radius specimens.<sup>26, 28</sup> Moreover, on bone mimicking phantoms covered by a soft tissue mimicking layer, <sup>13, 24, 42, 43</sup> indicate that the measured guided modes can be interpreted using a free plate model. Thus, an elastic plate model with a linear varying thickness, although it represents a simplification compared to the complex structure of bone, is adopted here in order to evidence the effect of the thickness variation on the guided mode measurement.

#### B. Adiabatic guided modes

The slowly varying thickness is associated with guided modes that are supposed to be adiabatic: they locally correspond to guided modes of a plate of constant thickness. If k(e, f) is a valid frequency-wavenumber curve for a free elastic plate whose thickness is e, then the frequency-wavenumber curve  $k(\alpha e, f)$  for a plate of any thickness  $\alpha e$  can be deduced using the equation

132 
$$k(\alpha e, f) = 1/\alpha \ k(e, \alpha f), \tag{1}$$

where  $\alpha$  is a generic waveguide thickness scaling factor. The two wavenumbers given in Eq. (1) correspond to identical frequency  $\times$  thickness and wavenumber  $\times$  thickness products. They also correspond to identical phase velocity and group velocity.

Consider two close positions x and x + dx along the waveguide that are associated with thicknesses such that e(x + dx) is equal to e(x) + de [Fig. 1(a)]. In order to discuss the expression given by Eq. (1), two particular plate modes A1 and S2 are illustrated on Figs. 1(b) and (c). The transition from the modes k(x, f) associated with the largest thickness e(x) (shown as thick lines) to the modes k(x + dx, f) associated with the smallest thickness e(x) + de (de chosen negative in this example, dashed lines) ) is manifested as a shift of the dispersion curves towards higher frequencies. An opposite effect, i.e. a shift towards lower frequencies, is observed when the thickness increases (positive de). Figure 1(c) is a zoom of a small portion of the (f, k) 2-D space shown in figure 1(b) indicating the small variations df, dk and  $\Delta k$  defined in Eqs. (3) and (4).

The scaling factor  $\alpha$  equal to e(x + dx) / e(x) can be expressed as 1 + de/e(x). The ratio de/e(x) is assumed to be small compared to 1 and thus further calculus will be done with the perturbation method at the first order of the quantity de/e(x). Equation (1) can be written as

149 
$$k(x + dx, f) = k(x, f - df) + dk.$$
 (2)

The previous equation links two wavenumbers for two different positions x and x + dx at two different frequencies, f and f - df. The small variations df and dk, induced by the thickness variation de, satisfy

$$df = -f \frac{de}{e(x)}, (3a)$$

154 
$$dk = -k(x, f)\frac{de}{e(x)}.$$
 (3b).

The first order Taylor expansion along frequency of wavenumber k(x, f - df) [right hand part of Eq. (2)] writes as

157 
$$k(x, f - df) = k(x, f) - \frac{\partial k}{\partial f} df.$$
 (4)

Using Eq. (3) and the definition of the phase and group velocities  $v_{\phi}$  and  $v_{g}$ , the derivative

159 term  $\frac{\partial k}{\partial f}df$  can be approximated by  $\frac{v_{\phi}(x,f)}{v_{g}(x,f)}dk$ . This term is shown as  $\Delta k$  on Fig. 1(c).

- 160 Combining Eqs. (2) to (4), the difference between k(x, f) and k(x + dx, f), illustrated as a thick
- arrow on Fig. 1(c), is equal to  $dk \Delta k$ . Finally, the variation of the wavenumber at a fixed
- 162 frequency writes

$$163 k(x+dx,f) = k(x,f) \left[ 1 + \frac{de}{e(x)} \left( \frac{v_{\phi}(x,f)}{v_{g}(x,f)} - 1 \right) \right]. (5)$$

Next, we introduce the term  $\varepsilon(x, f)$  defined as

165 
$$\varepsilon(x,f) = \frac{de}{e(x)} \left( \frac{v_{\phi}(x,f)}{v_{g}(x,f)} - 1 \right). \tag{6}$$

This term is dimensionless and can be interpreted as a deviation rate measuring the wavenumber variation in response to the thickness variation. Hereafter it will be referred to as the "deviation term". It depends on the waveguide thickness variation rate de/e(x), on the guided mode being considered and on its velocity dispersion.

#### C. Adiabatic condition

The "adiabatic condition", introduced in paragraph II.A, is satisfied if the deviation term  $\varepsilon(x, f)$ , given by Eq. (6), is small compared to 1. This case is satisfied for moderate dispersion and weak thickness variation. If mode dispersion is large, *i.e.*  $v_{\phi}$  is large compared to  $v_g$ , *e.g.*, for frequencies close to cut-off frequencies,  $\varepsilon$  could be non negligible even if the thickness variation de/e(x) is small. On the contrary, if mode dispersion is null, *i.e.*  $v_g$  and  $v_{\phi}$  are equal,  $\varepsilon$  is null and the thickness variation has not effect on the wavenumber. This is the case for example for the Rayleigh wave which corresponds to a surface wave and is not influenced by the opposite interface. Moreover, the dispersion term  $v_{\phi} / v_g - 1$  is mostly

positive. It implies that de and  $\varepsilon$  have the same sign: thus, an increase (respectively a decrease) in thickness leads to an increase (respectively a decrease) in the wavenumber. Exceptions are mode A0, for which  $v_g$  is inferior to  $v_\phi$ , and modes associated with ZGV (zero group velocity) resonances, for which group and phase velocities have opposite signs.<sup>44</sup>

Consider that the adiabatic condition is satisfied along the propagation path of n close positions  $x_i$  shown in Fig. 1(a), associated with n local thicknesses  $e(x_i)$ . At a fixed frequency f, along its propagation the wavenumber k(x, f) undergoes a series of homothetic transforms given by Eqs. (5) and (6). The n<sup>th</sup> position is linked to the first one with the following relationship

190 
$$k(x_n, f) = k(x_1, f) \prod_{i=1}^{n-1} \{1 + \varepsilon(x_i, f)\},$$
 (7)

with *i* the position index ranging from 1 to *n* [Fig 1(a)]. As all the deviation terms  $\varepsilon$  are assumed to be small compared to 1, the previous equation can be approximated to the first order in  $\varepsilon(x_i, f)$  with

194 
$$k(x_n, f) = k(x_1, f) \left\{ 1 + \sum_{i=1}^{n-1} \varepsilon(x_i, f) \right\}.$$
 (8)

At each step, a small variation  $\varepsilon(x_i, f).k(x_1, f)$  is added to the reference wavenumber  $k(x_1, f)$ . The measurement of the spatial variations of the wavenumber has been proposed to reconstruct the profile variation de(x) of the waveguide in case of moderate dispersion.<sup>45</sup>

## D. Wavenumber variation for a linearly varying thickness waveguide

Consider a linear array with a group of receivers surrounded with two groups of transmitters. The array is in contact with a waveguide with a linearly varying thickness (Fig. 2). The receivers are equally spaced, with an array pitch denoted p. The reference of axis (Ox), i.e. the position x = 0, is located at the center of the receiving array. This position is associated with the reference thickness  $e_0$ . Thus, the varying thickness e(x) is given by

$$e(x) = e_0 + x \cdot \tan \alpha \,, \tag{9}$$

with the subscript 0 associated with values at position x = 0. Notation "+" (respectively "-") denotes the increasing (respectively decreasing) thickness direction. By convention, the first receiver is placed on the thickest side, *i.e.*, at a negative position (Fig. 2). The variation of the wavenumbers along the receivers at a fixed frequency can be obtained using Eq. (7), as long as the adiabatic condition  $\varepsilon << 1$  [Eq. (6)] is satisfied at each adiabatic transform, *i.e.*, from one receiver to the next one in this case. Moreover, the variation of the wavenumber can be expressed as

213 
$$k(x,f) = k(x_0,f) \left( 1 + \frac{\varepsilon(x_0,f)}{p} x \right), \tag{10}$$

The term  $\varepsilon(x_0, f)$ , being the deviation term at the array center, is given by Eq. (6). In order to discuss the validity of Eq. (10), two frequencies, corresponding to two different deviation terms  $\varepsilon(x_0, f)$ , respectively, are considered in the following.

Examples are given in Fig. 3 for two modes, A1 and S2 shown in Fig. 1, propagating at frequencies of interest in a bone-mimicking wedged plate with an angle  $\alpha = 2^{\circ}$  and a thickness  $e_0 = 2.25$  mm. The geometrical characteristics of the wedged plate are representative of the typical values estimated from Ref. 16. The typical thickness variation de/e(x), equal to  $p\tan(\alpha)/e_0$ , is about 1.4 %, with p = 0.892 mm. Figure 3(a) shows first the dispersion curves  $k(x_0, f)$  of this plate at x = 0. The corresponding variations of the deviation terms  $\varepsilon(x_0, f)$  are shown in Fig. 3(b). Two selected frequencies are marked with symbols in Figs. 3(a) and (b). The first case marked with a star (mode A1 at  $f_1$  equal to 0.8 MHz), corresponds to a deviation term  $\varepsilon(x_0, f_1)$  equal to 0.9 %. The second case marked with a circle (mode S2 at  $f_2$  equal to 0.8 MHz), is associated with a more pronounced deviation term  $\varepsilon(x_0, f_2)$  equal to 7.7 %. Finally, figures 3(c) and (d) show the variation in x of the wavenumbers  $k(x, f_1)$  and  $k(x, f_2)$  and their corresponding amplitudes  $sin[k(x, f_1) x]$  and  $sin[k(x, f_2) x]$  for the two modes at the two

selected frequencies  $f_1$  and  $f_2$ . The receiver positions are marked with black dots.

It can be observed that both wavenumbers  $k(x, f_1)$  and  $k(x, f_2)$  decrease in the direction of decreasing thickness (direction "–"). On the contrary, for the opposite direction "+", *i.e.*, when thickness increases, the wavenumbers increase. Moreover, the variation of the wavenumbers along the axis (Ox) are well described by the linear approximation, given by Eq. (10) and shown with thin lines, even for the deviation  $\varepsilon(x_0, f_2) = 7.7$  %. These modes with varying wavenumber can be seen as being spatially modulated, as for example classical chirps, but in the spatial domain instead of the temporal domain [Fig. 3(d)].

## III. Material and methods

#### A. Experimental set up

The axial transmission setup is composed of a 1 MHz-centre frequency cMUT ultrasonic array (Vermon, Tours, France), a multi-channel array controller (Althaïs, Tours, France) and a custom made graphic interface. The cMUT array has been described in Ref. 46. Its configuration is detailed in Fig. 2: it consists of two sets of 5 transmitters on each side of a group of 24 receivers located at the centre of the array. This array with its two sets of transmitters was initially designed for soft tissues bidirectional correction.  $^{10,42}$  In the present work, this configuration allows waves propagation to be studied in both opposite directions, denoted "+" and "-" in Fig. 2. The array is controlled by the array controller and the graphic interface allows real-time visualization of the calculated (f - k) diagrams. The pitch of the elements, denoted p, is equal to 0.892 mm. The frequency bandwidth of the emitted signal, a one period burst of 1MHz corresponds to a -6 dB power spectrum spanning the frequency range of 0.5 to 1.6 MHz. Signals are recorded at a sampling frequency of 20 MHz and a 12-bit resolution with 16 time averages. The signals corresponding to all possible transmit-receive pairs in the array are recorded. The probe is placed in contact with the wedged plate using a

coupling gel (Aquasonic, Parker Labs, Inc, Fairfield, NJ, USA).

The bone-mimicking plate is made of glass fibres embedded in epoxy (Sawbones Pacific Research Laboratories, Vashon, WA, USA). The following mechanical properties, <sup>47</sup> obtained with resonant ultrasound spectroscopy, <sup>48</sup> were used to compute the guided wave dispersion curves in the bone-mimicking plate using a 2-D transverse isotropic free plate model: <sup>24, 25, 49</sup> mass density 1.64 g.cm<sup>-3</sup> and stiffness coefficients (in GPa)  $c_{11} = 13.9$ ;  $c_{33} = 20.9$ ;  $c_{55} = 4.3$ ;  $c_{13} = 6.9$ . The guided modes are labelled An and Sn considering their symmetry and their apparition order in frequency. In the following, measurements were performed on a bone-mimicking wedged plate, the angle of which is denoted  $\alpha$ . Two wedged plates with  $\alpha$  equal to 1° and 2° were measured. A plate without angle was also measured as a reference.

## **B. SVD-based signal processing**

The experimental setup described in section III.A allows the measurement of 2 sets of  $M \times N$  temporal signals, each of which consisting of all the signals that correspond to one of the 2 directions of propagation. M and N are the number of receivers and transmitters, respectively. Waveguides with varying thickness have been already studied in non-destructive evaluation (NDE), where materials generally have light damping and large dimensions compared to the wavelength. Thus, large propagation paths can be recorded and analyzed using a standard post-processing technique, the so-called spatio-temporal Fourier transform,  $^{50}$  with the assumption that the thickness of the waveguide remains constant along the receiving aperture.  $^{35, 36}$  Time-frequency analysis  $^{33, 36}$  and analysis of the reflection coefficient  $^{39}$  have also been proposed. Correction in the time domain have been recently investigated to compensate the pulse dispersion caused by a varying thickness.  $^{51}$  In contrast to the materials investigated in NDE, cortical bone and specifically the bone mimicking material investigated here are highly damping materials. The combination of absorption and of the limited

receiving length of the array makes that specific signal processing is therefore required to enhance the wavenumber evaluation.

A SVD-based signal processing technique was recently developed for this purpose and has been extensively detailed in our previous publications.<sup>11, 23</sup> Briefly, it takes advantage of the multi-transmit, multi-receive configuration of the ultrasonic array. If  $s_{nm}(t)$  denotes the temporal signal recorded at the receiver positioned at  $x_m^R$  after transmission by the  $n^{th}$  transmitter, the main steps of the SVD-based signal processing can be summarized as follows:

- 1) computation of the temporal Fourier transform  $S_{nm}(f)$  of the N by M responses  $S_{nm}(f)$ .
- 2) singular value decomposition of the transfer matrix S at each frequency: S is decomposed on N reception singular vectors  $U_n$ , and we denote by  $\sigma_n$  the associated singular value.
- 3) separation of signal from noise by identifying the singular values larger than a heuristically determined threshold, and by keeping only the corresponding number of singular vectors. This sets the rank of the matrix **S** at each frequency.
- 4) definition of appropriate test vectors  $\mathbf{e}^{test}$  with a norm equal to 1, expressed in the receivers basis. The projection of these test vectors onto the signal subspace (*i.e.* the reception singular vectors) leads to the so-called normalized *Norm* function, defined by  $^{11,23}$

298 
$$Norm(f,k) = \sum_{n=1}^{rank} \left| \left\langle \mathbf{U}_n \left| \mathbf{e}^{test} \right\rangle \right|^2.$$
 (11)

5) extraction of the guided mode wavenumbers corresponding to the maxima of the *Norm* function. To this end, a second threshold is heuristically defined.

These operations are performed on matrices of signals recorded with both sets of transmitters, so that two *Norm* functions are calculated, one for each propagation direction. This signal processing technique significantly enhances the identification of the branches in the f - k

diagrams, for two reasons: first, the signal is separated from noise; second, the matrix *Norm* is normalized, *i.e.* all points have their values between 0 and 1. The maxima values do not depends on the mode energy. Maxima of the *Norm* function close to 1 mean that the testing vector is close to a measured mode.

However, the choice of the test vectors is critical to enhance the guide mode wavenumber measurement. In Ref. 11, the test vectors are plane waves

$$e_m^{test}(k) = \frac{1}{\sqrt{M}} e^{ikx_m^R}, \qquad (12)$$

where k is a wavenumber corresponding to a plane wave. These test vectors are appropriate for modes propagating in a waveguide of constant thickness. Indeed, the projection of plane waves onto the basis of the singular vectors is equivalent to performing the spatial Fourier transform of the singular vectors. The method has been extended to dissipative waveguides by using a complex wavenumber. While this approach is appropriate for modes propagating in a waveguide of constant thickness, the developments presented in section II indicate that the approach may no longer be adapted in case of a thickness-varying waveguide.

## C. Test vector with varying wavenumber

Paragraph II.C shows that the wavenumbers of the guided modes is affected by changes in the thickness of the waveguide. However, in the current SVD-based signal processing, the test vectors include a constant wavenumber. It may be preferable to use test vectors that fit better the physics of the problem. Towards this goal, the plane waves [Eq. (12)] are replaced by waves with a varying wavenumber following

326 
$$e_m^{test}(k,\varepsilon) = \frac{1}{\sqrt{M}} e^{ik^{test}(x_m^R)x_m^R}, \tag{13}$$

with  $k^{test}(x)$  defined with coefficients k and  $\varepsilon$  of a first order Taylor expansion following

Eq. (10) as

329 
$$k^{test}\left(x\right) = k\left(1 + \frac{\varepsilon}{p}x\right). \tag{14}$$

330 The example of a simple case of a single propagating mode associated with a single singular vector  $\mathbf{U}_1$  is given to illustrate this adaptation of the signal processing. The singular vector is defined using Eqs. (10) and (14) with two arbitrary values  $k_0$  and  $\varepsilon_0$ . In this case, the scalar product  $\langle \mathbf{e}^{\text{test}}(k, \varepsilon) | \mathbf{U}_1 \rangle$  writes as

334 
$$\left\langle \mathbf{e}^{test}\left(k,\varepsilon\right)\middle|\mathbf{U}_{1}\right\rangle = \frac{1}{M}\sum_{m=1}^{M}\exp\left[i\left(\left(k_{0}-k\right)+\left(k_{0}\frac{\varepsilon_{0}}{p}-k\frac{\varepsilon}{p}\right)x_{m}^{\mathrm{R}}\right]x_{m}^{\mathrm{R}}\right].$$
 (15)

335 The *Norm* function [Eq. (11)] expresses as

336 
$$Norm(k,\varepsilon) = \left| \left\langle \mathbf{e}^{test}(k,\varepsilon) | \mathbf{U}_1 \right\rangle \right|^2.$$
 (16)

## D. Comparison with the spatial Fourier transform and validity domain

The two examples shown in Fig. 3 are discussed. They correspond to guided waves propagating in a bone-mimicking wedged plate with an angle  $\alpha=2^{\circ}$  and a thickness  $e_0=2.25$  mm. The propagation of modes A1 and S2 was computed using Eq. (7) at a frequency of 0.8 MHz. In the first example, the propagation of mode A1 is investigated. It is represented with a star in the figures, and one can see that it corresponds to  $\varepsilon_0=0.9$  % and  $k_0=1.5$  rad.mm<sup>-1</sup>. This is considered to be a moderate wavenumber variation between the first and the last receivers, the term  $M\varepsilon_0k_0$  having a value of about 0.2 rad.mm<sup>-1</sup> [Eq. (10)]. In the second example, we consider the propagation of mode S2, represented with a circle in the figures. Although the frequency is the same as for mode A1, in this case  $\varepsilon_0=7.7$ % and  $k_0=0.5$  rad.mm<sup>-1</sup>. This corresponds to a larger wavenumber variation of about 1 rad.mm<sup>-1</sup>. The spatial Fourier transform of these two examples is shown in Figs. 4(a) and (b) with a thick gray line. In the first example (mode A1), the peak is located at  $k=k_0$ , and thus the corresponding moderate wavenumber variation does not affect the ability of the spatial

Fourier transform to evaluate the wavenumber at the center of the array. On the other hand, in the second example (mode S2), the spatial Fourier transform exhibits two maxima that are shifted compared to the pick value located at  $k_0$ . Thus, the larger wavenumber variation prevents the evaluation of an accurate estimate of the wavenumber. In the single mode case discussed here, the spatial Fourier transform corresponds to the plane wave test vectors [Eq. (12)] as described in Ref. 11. It is then calculated with  $\varepsilon = 0$  in Eq. (16) and therefore it is indicated as Norm(k, 0) in Figs. 4(a) and (b).

In order to illustrate the signal processing using a modified test vector [Eqs. (13) to (16)], the *Norm* function is shown in the  $(k, \varepsilon)$  plane in Figs. 4(c) and (d). The *Norm* function presents a single peak centered at the point  $(k_0, \varepsilon_0)$ , shown with a star (A1) and a circle (S2). In order to compare with the spatial Fourier transform, the line corresponding to  $\varepsilon = \varepsilon_0$  is shown as a thin black line, and is indicated as  $Norm(k, \varepsilon_0)$  in Figs. 4(a) and (b). It can be observed that the value of the maxima is 1. A maximum value close to 1 suggests that the correction proposed in Eq. (14), using the modified test vector, has succeeded to compensate for the wavenumber variation due to the varying thickness.

The measurement limit domains are indicated with thick lines. The lowest measurable wavenumber,  $\pi/L$ , corresponds to a wavelength equal to half the extent of the receiving area equal to L or Mp. The highest measurable wavenumber,  $2\pi/p$ , corresponds to the sampling wavenumber, denoted  $k_s$ . In this case, the wavelength is equal to the array pitch p. Indeed, as the guided modes are recorded in only one propagation direction, the measured wavenumber have only one (positive) sign and thus the Nysquist limit (k inferior to  $k_s/2$ ) can be exceeded until k equal to  $k_s$ . The line  $\varepsilon = 10$  % corresponds to the upper limit of the adiabatic condition discussed in paragraph II.C. Thus below 10%, the deviation term  $\varepsilon(x,f)$  given by Eq. (6) is considered small compared to 1, and the linear variation of the wavenumber [Eq. (10)] is valid.

377 The resolution is given by the mid peak values. Resolutions in k and  $\varepsilon$ , denoted  $\delta k$  and 378  $\delta \varepsilon$ , respectively, are equal to

$$\delta k = 2\pi/L,\tag{17}$$

$$\delta \varepsilon = 4\pi/(M k_0 L) \,, \tag{18}$$

These values are illustrated in Fig. 4 with horizontal and vertical thin arrows around the peaks. The resolution  $\delta k$  is the same as in the case of the plane wave test vectors and depends only on the receiving length L. In addition to L, the resolution  $\delta \varepsilon$  depends on the wavenumber  $k_0$  and the number of receivers M. The domain of validity is divided into two zones, denoted I and II. If the couple  $(\varepsilon_0, k_0)$  is located in zone I, the associated peak intercepts the  $\varepsilon = 0$  line. Thus following Eq. (18), the limit between the two zones corresponds to  $\varepsilon k$  less than  $4\pi/(ML)$ . Thus in zone I, is it possible to localize the position of the maxima (i.e.,  $k = k_0$ ) using the spatial Fourier Transform as illustrated with the A1 mode. The peaks given by the two methods are located at the same wavenumbers equal to  $k_0$ , but the peak maximum given by the spatial Fourier transform is lower than the value given by the proposed method (about 0.8 instead of 1). On the contrary, if the couple  $(\varepsilon_0, k_0)$  is located in zone II, i.e.,  $\varepsilon_0 k_0$  larger than  $4\pi/(ML)$ , then the peak does not intercept the  $\varepsilon = 0$  line and therefore it is not possible to localize the maxima using the spatial Fourier Transform as illustrated with the S2 mode. However, the correction proposed in Eq. (14), allows the detection of the modes, even in zone II as long as the deviation term is less than 10 %, and the function  $Norm(k, \varepsilon)$  exhibits a unique peak associated with a maximum value close to 1 and located at  $(k_0, \varepsilon_0)$ .

In conclusion, these examples illustrate that the proposed approach where the plane wave vector has been changed to a test vector with a varying wavenumber leads to a better mode detection, and consequently to a more accurate wavenumber measurement.

381

382

383

384

385

386

387

388

389

390

391

392

393

394

395

396

397

398

399

400

## IV. Results and discussion

In this section, experimental data are collected on three wedged plates made of bone-mimicking material. The thickness  $e_0$  of the plates at the center of the receiving area is equal to 2.25 mm. The wedge angles  $\alpha$  are equal to 0, 1 and 2°. All calculations have been done keeping the five singular vectors [*i.e.*, the rank is equal to 5 in Eq. (11)] and with a second threshold equal to 0.6. Whereas the *Norm* function computed with a plane wave test vector depends on two parameters (f, k) using the plane wave test vector [Eq. (12)], the new *Norm* function computed with a test vector with varying wavenumber [Eqs. (13) and (14)] depends on the three parameters f, k and  $\varepsilon$ . The results are represented in Fig. 5 for the bone-mimicking wedged plates with a wedge angle  $\alpha = 1^\circ$  [Fig. 5(b) and (c)] and  $\alpha = 2^\circ$  [Fig. 5(d) and (e)]. Results calculated with the modified test vector k (circles) are compared with those obtained with the plane wave test vector (dots) for both directions "+" and "–". The case of the plate of constant thickness ( $\alpha = 0^\circ$ ), is shown in Fig. 5(a) for reference. The main observations are as follows:

- Incomplete portions of branches of guided modes are detected in the wedged plates
   compared to the plate of constant thickness.
- 418 2. This effect is more pronounced in the direction "+" compared to the opposite direction.
- 3. The length of the detected branches with the plane wave test vector decreases when the angle increases.
  - 4. Several branches of guided modes in the wedged plates that are incompletely detected with the plane test vector (e.g., S0, A3 plate with  $\alpha = 1^{\circ}$ , direction "-"; S0, A1, S1, A3 plate with  $\alpha = 1^{\circ}$ , direction "-") can be detected using the modified test vector. Guided mode branches measured only with the modified method are indicated with thin arrows. It corresponds to wavenumbers located in zone II of Fig. 4.

5. Some modes are even not detected at all (e.g., A3; directions "+") with either the plane wave or modified test vector. Guided mode branches not measured with any of the two methods are marked with thick black arrows.

Results are now discussed in details. Five guided modes are measured in the reference case [Fig. 5(a)]. The two first modes A0 and S0 do not have cut-off frequencies unlike the three following modes A1 (0.4 MHz), S2 (0.7 MHz) and A3 (1.3 MHz). Modes A2 and S3 are not measured. Let us consider first the results obtained with the plane wave test vectors (dots). Direction "+" (right panels) is more severely affected compared to direction "-". At 1°, the mode A3 is no longer detected. For modes A1 and S2, low wavenumbers with values below 0.5 rad.mm<sup>-1</sup>, are missing. The mode A1 also disappears at high wavenumbers, with values above 2 rad.mm<sup>-1</sup>. For the 2° wedged plate, in addition to the mode A3, the mode S2 also completely disappears. The mode A1 is not measured for wavenumbers below 1 rad.mm<sup>-1</sup>. For direction "-" (left panels), similar but less important alterations of the branches can be observed. For example, at 1°, A3 is partially detected while A1 and S2 seem to be correctly detected. At 2°, A3 is no longer detected and S2 is partially detected. For high wavenumbers, modes S0 and A1 are not detected. Mode A0 is the only mode that does not seem to be affected for both directions.

Some branches of guided modes that are not detected with the plane test vector can be measured using the modified test vector  $k^{\text{test}}(x)$  [Eq. (14)]. These branches are indicated with thin arrows. This effect is particularly visible for the 2° wedged plate and direction "–" [Fig. 5(d)] on modes S0, A1, S2, A3. Almost all branches lost using the plane test vector can be recovered. Similar effect is observed for the 2° wedged plate and direction "+" [Fig. 5(e)]. Note that mode A3 cannot be measured in both wedged plates with any of the two methods.

These observations are in agreement with the comments of Figs. (3) and (4). First, the

effect of the varying thickness increases with the wedge angle and with mode dispersion. Remember that the mode dispersion is high close to cut off frequencies, particularly for modes S2 and A3. The effect also increases with the wavenumber values as observed for modes S0 and A1. Secondly, the observation of direction "+" being more affected than direction "-" can be interpreted by the fact that, the plate being too thin under the transmitters, some modes such as S2 and A3 cannot be excited and subsequently cannot be measured by the receivers. On the contrary, for direction "-", these modes are excited under the transmitters and can propagate and can be measured. However these modes may vanish before the end of the receiving length, as for example S2 at 0.8 MHz and x about 10 mm [Fig. 3(c)]. This is similar to the phenomenon described as "acoustic black holes" for the flexural waves propagating in wedges with thickness decreasing with a power law exponent larger than 2.52 Moreover in our case, as the bone-mimicking material is absorbing, no reflections are observed.

Using the modified test vector allows the estimation not only of the wavenumbers as discussed above, but also of the deviation term  $\varepsilon$  as shown in Fig. 4. The theoretical value of  $\varepsilon(x_0, f)$  is plotted versus frequency for modes A1, S1 and A3 in Fig. 6 for both angles  $\alpha = 1$  and  $\alpha = 2^{\circ}$ . Experimental values (shown with symbols), measured in direction "—", are compared to the theoretical ones, showing good agreement for both plates. The experimental deviation term  $\varepsilon$  is slightly underestimated. Moreover, close to cut off frequencies, the detection of the maxima can become unstable because the dispersion term  $v_{\phi}/v_{g}$ —1 tends towards infinity. This suggests that the limit to the linear approximation for the variations of the wavenumbers is  $\varepsilon$  of the order of 10 % (Fig. 4). Above this value, the test vectors defined in Eq. (14) are not adapted anymore and another type of variation should be considered (e.g. polynomial approximation of higher order). Attenuation could be also taken into account as the imaginary part of the wavenumber also varies spatially.

Given the relatively low signal-to-noise ratio in axial transmission measurements of cortical bone, we believe that the improvement in the detection of branches brought by the modified version of the test vector may represent a significant progress. Moreover, previous results suggest that direction "–" is potentially better for cortical bone characterization. As a consequence, further assessment of the method on *ex vivo* specimens as well as in *in vivo* measurement conditions is warranted.

#### V. Conclusion

This paper introduces a modified signal processing approach adapted to the measurement of guided wave propagation in waveguides of variable thickness. The method is based on an equation that describes the evolution of the guided modes wavenumbers with respect to position along the direction of propagation in the wedged plate. Both the equation and the signal processing were validated using experimental data recorded with bone-mimicking wedged plates. This new approach to detect guided waves in wedged plates exhibits enhanced sensitivity and accuracy compared to the previous one that does not account for the thickness-related variations of the wavenumbers. Indeed, typical angles of approximately 1° to 2° observed in the cortical layer of the radius affect the propagation of the guided waves and prevent large parts of the guided mode branches to be detected with the current signal processing. The modified signal processing has therefore a better potential for investigation of the inverse problem aiming at retrieving estimates of thickness and elastic properties of the cortical bone waveguide.

## Acknowledgments

This work was supported by the ANR grant COSTUM 09-TECS-005-03 (2009-2012).

Moreau *et al*.

Authors would like to acknowledge Pascal Dargent for his help for preparing the wedged plates.

Jean-Gabriel Minonzio would like to dedicate the paper to the memory of Franck David Philippe who passed away during the preparation of the manuscript.

507

- 508 1. P. Moilanen, "Ultrasonic guided waves in bone," IEEE Trans. Ultrason. Ferroelectr.
- 509 Freq. Control **55**, 1277–1286 (2008).
- 510 2. M. Talmant, J. Foiret, and J. G. Minonzio, Bone Quantitative ultrasound Chap. 7
- 511 Guided waves in cortical bones (Springer, New York, 2010).
- 3. R. M. D. Zebaze, A. Ghasem-Zadeh, A. Bohte, S. Iuliano-Burns, M. Mirams, R. I.
- Price, E. J. Mackie, and E. Seeman, "Intracortical remodelling and porosity in the
- distal radius and post-mortem femurs of women: a cross-sectional study," Lancet 375,
- 515 1729–1736 (2010).
- 516 4. P. Laugier, "Instrumentation for in vivo ultrasonic characterization of bone strength,"
- 517 IEEE Trans. Ultrason. Ferroelectr. Freq. Control **55**, 1179–1196 (2008).
- 518 5. P. Moilanen, P. H. F. Nicholson, T. Karkkainen, Q. Wang, J. Timonen, and S. Cheng,
- "Assessment of the tibia using ultrasonic guided waves in pubertal girls," Ost. Int. 14,
- 520 1020–1027 (2003).
- 521 6. D. Ta, W. Q. Wang, Y. Y. Wang, L. H. Le, and Y. Q. Zhou, "Measurement of the
- Dispersion and Attenuation of Cylindrical Ultrasonic Guided Waves in Long Bone,"
- 523 Ultrasound Med. Biol. **35**, 641–652 (2009).
- 524 7. K. L. Xu, D. Ta, P. Moilanen, and W. Q. Wang, "Mode separation of Lamb waves
- based on dispersion compensation method," J. Acoust. Soc. Am. 131, 2714–2722
- 526 (2012).
- 527 8. X. J. Song, D. A. Ta, and W. Q. Wang, "A Base-Sequence-Modulated Golay Code
- Improves the Excitation and Measurement of Ultrasonic Guided Waves in Long
- Bones," IEEE Trans. Ultrason. Ferroelectr. Freq. Control **59**, 2580–2583 (2012).
- 530 9. A. Tatarinov, V. Egorov, N. Sarvazyan, and A. Sarvazyan, "Multi-frequency axial
- 531 transmission bone ultrasonometer," Ultrasonics,

- 532 http://dx.doi.org/10.1016/j.ultras.2013.09.025 (date last viewed 02/20/14).
- 533 10. E. Bossy, M. Talmant, M. Defontaine, F. Patat, and P. Laugier, "Bidirectional axial
- transmission can improve accuracy and precision of ultrasonic velocity measurement
- in cortical bone: A validation on test materials," IEEE Trans. Ultrason. Ferroelectr.
- 536 Freq. Control **51**, 71–79 (2004).
- 537 11. J. G. Minonzio, M. Talmant, and P. Laugier, "Guided wave phase velocity
- measurement using multi-emitter and multi-receiver arrays in the axial transmission
- configuration," J. Acoust. Soc. Am. **127**, 2913–2919 (2010).
- 540 12. P. Moilanen, M. Maatta, V. Kilappa, L. Xu, P. H. F. Nicholson, M. Alen, J. Timonen,
- T. Jamsa, and S. Cheng, "Discrimination of fractures by low-frequency axial
- transmission ultrasound in postmenopausal females," Ost. Int. **24**, 723–730 (2013).
- 543 13. P. Moilanen, Z. Zhao, P. Karppinen, T. Karppinen, V. Kilappa, J. Pirhonen, R.
- Myllylä, E. Hæggström, and J. Timonen, "Photo-acoustic Excitation and Optical
- Detection of Fundamental Flexural Guided Wave in Coated Bone Phantoms,"
- 546 Ultrasound Med. Biol. **40**, 521–531 (2014).
- 547 14. G. Lowet and G. VanderPerre, "Ultrasound velocity measurement in long bones:
- Measurement method and simulation of ultrasound wave propagation," J.
- 549 Biomechanics **29**, 1255–1262 (1996).
- 550 15. M. Daugschies, K. Rohde, C.-C. Glüer, and R. Barkmann, "The preliminary
- evaluation of a 1 MHz ultrasound probe for measuring the elastic anisotropy of human
- 552 cortical bone," Ultrasonics **54**, 4–10 (2014).
- 553 16. E. Bossy, M. Talmant, F. Peyrin, L. Akrout, P. Cloetens, and P. Laugier, "An in vitro
- study of the ultrasonic axial transmission technique at the radius: 1-MHz velocity
- measurements are sensitive to both mineralization and intracortical porosity," J. Bone
- 556 Mineral Res. **19**, 1548–1556 (2004).

557 17. J. Foiret, Q. Grimal, M. Talmant, R. Longo, and P. Laugier, "Probing heterogeneity of

- cortical bone with ultrasound axial transmission," IEEE Trans. Ultrason. Ferroelectr.
- 559 Freq. Control **60**, 187–193 (2013).
- 560 18. K. I. Lee and S. W. Yoon, "Correlations between ultrasonic guided wave velocities
- and bone properties in bovine tibia in vitro," J. Acoust. Soc. Am. 131, EL375–EL381
- 562 (2012).
- 563 19. A. Sarvazyan, A. Tatarinov, V. Egorov, S. Airapetian, V. Kurtenok, and C. J. Gatt,
- "Application of the dual-frequency ultrasonometer for osteoporosis detection,"
- 565 Ultrasonics **49**, 331–337 (2009).
- 566 20. V. Egorov, A. Tatarinov, N. Sarvazyan, R. Wood, L. Magidenko, S. Amin, S. Khosla,
- R. J. Ruh, J. M. Ruh, and A. Sarvazyan, "Osteoporosis detection in postmenopausal
- women using axial transmission multi-frequency bone ultrasonometer: Clinical
- findings," Ultrasonics, http://dx.doi.org/10.1016/j.ultras.2013.08.017 (date last viewed
- 570 02/20/14).
- 571 21. V. Kilappa, K. Xu, P. Moilanen, E. Heikkola, D. Ta, and J. Timonen, "Assessment of
- the Fundamental Flexural Guided Wave in Cortical Bone by an Ultrasonic Axial-
- 573 Transmission Array Transducer," Ultrasound Med. Biol. **39**, 1223–1232 (2013).
- 574 22. V. C. Protopappas, D. I. Fotiadis, and K. N. Malizos, "Guided ultrasound wave
- propagation in intact and healing long bones," Ultrasound Med. Biol. **32**, 693–708
- 576 (2006).
- 577 23. J. G. Minonzio, J. Foiret, M. Talmant, and P. Laugier, "Impact of attenuation on
- guided mode wavenumber measurement in axial transmission on bone mimicking
- 579 plates," J. Acoust. Soc. Am. **130**, 3574–3582 (2011).
- 580 24. J. A. Chen, J. Foiret, J. G. Minonzio, M. Talmant, Z. Q. Su, L. Cheng, and P. Laugier,
- "Measurement of guided mode wavenumbers in soft tissue-bone mimicking phantoms

- using ultrasonic axial transmission," Phys. Med. Biol. **57**, 3025–3037 (2012).
- 583 25. J. A. Chen, J. Foiret, J. G. Minonzio, Z. Q. Su, L. Cheng, and P. Laugier,
- "Corrigendum: Measurement of guided mode wavenumbers in soft tissueâ€"bone
- mimicking phantoms using ultrasonic axial transmission," Phys. Med. Biol. **58**, 8593–
- 586 8595 (2013).
- 587 26. J. Foiret, J. Minonzio, M. Talmant, and P. Laugier, "Cortical bone quality assessment
- using quantitative ultrasound on long bones," Engineering in Medicine and Biology
- Society (EMBC), Annual International Conference of the IEEE, 1121–1124 (2012).
- 590 27. J. Foiret, J.-G. Minonzio, P. Laugier, and M. Talmant, "Determination of bone
- properties from Lamb type of waves," POMA **19**, 075091 (2013).
- 592 28. P. Moilanen, P. H. F. Nicholson, V. Kilappa, S. Cheng, and J. Timonen, "Measuring
- guided waves in long bones: Modeling and experiments in free and immersed plates,"
- 594 Ultrasound Med. Biol. **32**, 709–719 (2006).
- 595 29. M. G. Vavva, V. C. Protopappas, L. N. Gergidis, A. Charalambopoulos, D. I. Fotiadis,
- and D. Polyzos, "Velocity dispersion of guided waves propagating in a free gradient
- elastic plate: Application to cortical bone," J. Acoust. Soc. Am. 125, 3414–3427
- 598 (2009).
- 599 30. A. Papacharalampopoulos, M. G. Vavva, V. C. Protopappas, D. I. Fotiadis, and D.
- Polyzos, "A numerical study on the propagation of Rayleigh and guided waves in
- cortical bone according to Mindlin's Form II gradient elastic theory," J. Acoust. Soc.
- 602 Am. **130**, 1060–1070 (2011).
- 603 31. P. Moilanen, P. H. F. Nicholson, V. Kilappa, S. L. Cheng, and J. Timonen,
- "Assessment of the cortical bone thickness using ultrasonic guided waves: Modelling
- and in vitro study," Ultrasound Med. Biol. **33**, 254–262 (2007).
- 606 32. V. Pagneux and A. Maurel, "Lamb wave propagation in elastic waveguides with

variable thickness," Proceedings of the Royal Society A: Mathematical, Physical and

- Engineering Science **462**(2068), 1315–1339 (2006).
- 609 33. L. De Marchi, A. Marzani, N. Speciale, and E. Viola, "Prediction of pulse dispersion
- in tapered waveguides," NDT & E International 43, 265–271 (2010).
- 611 34. N. Amir, V. Pagneux, and J. Kergomard, "A study of wave propagation in varying
- cross-section waveguides by modal decomposition .2. Results," J. Acoust. Soc. Am.
- **101**, 2504–2517 (1997).
- 614 35. M. E. C. El-Kettani, F. Luppe, and A. Guillet, "Guided waves in a plate with linearly
- varying thickness: experimental and numerical results," Ultrasonics 42, 807–812
- 616 (2004).
- 617 36. P. Marical, M. E. C. El-Kettani, and M. V. Predoi, "Guided waves in elastic plates
- with Gaussian section variation: Experimental and numerical results," Ultrasonics 47,
- 619 1–9 (2007).
- 620 37. Z. Hamitouche, M. E. C. El-Kettani, J. L. Izbicki, and H. Djelouah, "Reflection at the
- 621 Cut-off and Transmission by Tunnel Effect in a Waveguide with Linear Section
- Variation," Acta Acustica United with Acustica 95, 789–794 (2009).
- 623 38. J. B. Doc, S. Felix, and B. Lihoreau, "Coarse-grid computation of the one-way
- propagation of coupled modes in a varying cross-section waveguide," J. Acoust. Soc.
- 625 Am. **133**, 2528–2532 (2013).
- 626 39. R. Carandente, J. Ma, and P. Cawley, "The scattering of the fundamental torsional
- mode from axi-symmetric defects with varying depth profile in pipes," J. Acoust. Soc.
- 628 Am. **127**, 3440–3448 (2010).
- 629 40. J. M. Arnold and L. B. Felsen, "Intrinsic Modes in a Nonseparable Ocean
- 630 Waveguide," J. Acoust. Soc. Am. **76**, 850–860 (1984).
- 631 41. E. Bossy, M. Talmant, and P. Laugier, "Three-dimensional simulations of ultrasonic

axial transmission velocity measurement on cortical bone models," J. Acoust. Soc.

- 633 Am. **115**, 2314–2324 (2004).
- 634 42. L. Moreau, J. G. Minonzio, J. Foiret, E. Bossy, M. Talmant, and P. Laugier, "Accurate
- measurement of guided modes in a plate using a bidirectional approach," J. Acoust.
- 636 Soc. Am. **135**, EL15–EL21 (2014).
- 637 43. T. Tran, L. Stieglitz, Y. J. Gu, and L. H. Le, "Analysis of Ultrasonic Waves
- Propagating in a Bone Plate over Awater Half-Space with and without Overlying Soft
- Tissue," Ultrasound Med. Biol. **39**, 2422–2430 (2013).
- 640 44. C. Prada, D. Clorennec, and D. Royer, "Local vibration of an elastic plate and zero-
- group velocity Lamb modes," J. Acoust. Soc. Am. **124**, 203–212 (2008).
- 642 45. M. E. C. El Kettani, P. Marical, and Z. Hamitouche, "Inverse Problem for the
- Geometry Profile Determination of Waveguides With Varying Section Using
- Adiabatic Behavior of Guided Waves," IEEE Trans. Ultrason. Ferroelectr. Freq.
- 645 Control **56**, 2023–2026 (2009).
- 646 46. D. Certon, R. Ternifi, A. Boulme, M. Legros, J. G. Minonzio, M. Talmant, F. Patat,
- and J. P. Remenieras, "Low frequency cMUT technology: Application to
- measurement of brain movement and assessment of bone quality," IRBM **34**, 159–166
- 649 (2013).
- 650 47. S. Bernard, O. Grimal, S. Haupert, and P. Laugier, "Assessment of anisotropic
- elasticity of small bone samples with resonant ultrasound spectroscopy: Attenuation
- does not prevent the measurements," Ultrasonics Symposium (IUS), IEEE
- 653 International, 1599–1602, (2011).
- 654 48. S. Bernard, Q. Grimal, and P. Laugier, "Accurate measurement of cortical bone
- elasticity tensor with resonant ultrasound spectroscopy," Journal of the Mechanical
- Behavior of Biomedical Materials **18**, 12–19 (2013).

657 49. S. H. Rhee, J. K. Lee, and J. J. Lee, "The group velocity variation of Lamb wave in fiber reinforced composite plate," Ultrasonics **47**, 55–63 (2007).

- 659 50. D. Alleyne and P. Cawley, "A 2-Dimensional Fourier-Transform Method for the
- Measurement of Propagating Multimode Signals," J. Acoust. Soc. Am. **89**, 1159–1168
- 661 (1991).
- 51. L. De Marchi, A. Marzani, and M. Miniaci, "A dispersion compensation procedure to
- extend pulse-echo defects location to irregular waveguides," NDT & E International
- **54**, 115–122 (2013).
- 665 52. V. V. Krylov and F. J. B. S. Tilman, "Acoustic 'black holes' for flexural waves as
- effective vibration dampers," Journal of Sound and Vibration **274**, 605–619 (2004).
- 53. V. V. Krylov and R. Winward, "Experimental investigation of the acoustic black hole
- effect for flexural waves in tapered plates," Journal of Sound and Vibration 300, 43–
- 669 49 (2007).
- 670
- 671
- 672

Figure 1. X-ray computed tomography cross sections of a human distal radius (Siemens, Somaton 4 Plus) excerpted from Ref. 41, illustrating cortical bone thickness variations in a typical ultrasound measurement region (a), wavenumber k vs frequency f for two particular guided modes A1 and S2 (b) associated with the thickness e at position f (thick lines) and f and f are position f (thin lines), panel (c) is a zoom of (b) showing the small variations f and f and f and f and f used in Eqs. (3) to (6).

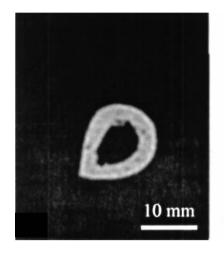
Figure 2. Configuration of the wedged plate with the elements of the ultrasonic array.

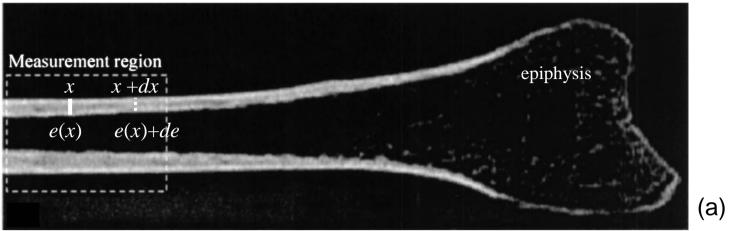
Figure 3. Wavenumbers  $k(x_0, f)$  of modes A1 and S2 vs frequency in a 2.25 mm-thick bone mimicking plate (a), corresponding deviation terms  $\varepsilon(x_0, f)$  [Eq. (6)] for  $\alpha = 2^{\circ}$  (b), wavenumbers  $k(x, f_1)$  and  $k(x, f_2)$  (c) and associated spatial variations  $sin[k(x, f_1)x]$  and  $sin[k(x, f_2)x]$  (d) of the two modes with respect to the propagation distance x at two particular frequencies shown with symbols for A1 at  $f_1 = 0.8$  MHz (star) and S2 at  $f_2 = 0.8$  MHz (circle) in (a) and (b) (points indicate the position of the receivers of the array).

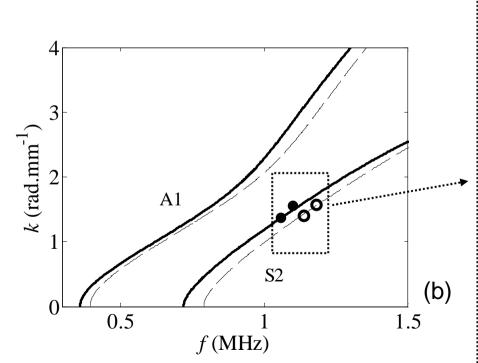
Figure 4. *Norm* functions given by Eq. (16) in the  $(k, \varepsilon)$  2-D space in a case of a single mode given by Eq. (10) for the two examples shown in Fig. 3: mode S2 at 0.8 MHz with  $\varepsilon_0$  equal to 7.7% and  $k_0$  equal to 0.5 rad.mm<sup>-1</sup> (a) and (c) and mode A1 at 0.8 MHz with  $\varepsilon_0$  equal to 0.9% and  $k_0$  equal to 1.5 rad.mm<sup>-1</sup> (b) and (d). The *Norm* functions are also represented for  $\varepsilon = 0$  (thick gray lines) and  $\varepsilon = \varepsilon_0$  (thin black lines) in (a) and (b). The case  $\varepsilon = 0$  corresponds to the previous signal processing using plane wave test vectors [Eq. (12)] and is equivalent to the spatial Fourier transform in the single mode case. The resolution values in the  $(k - \varepsilon)$  2-D space given by Eqs. (17) and (18) are shown with thin arrows. The thick lines corresponds to validity domains of zone I (spatial Fourier transform) and zone II (modified test vector).

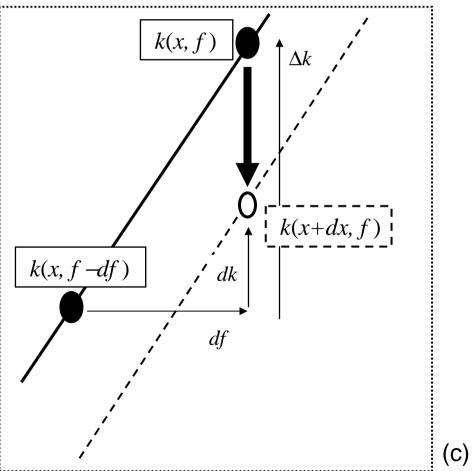
Figure 5. (color online) Experimental wavenumbers obtained with the plane wave test vector for a plate of constant thickness e=2.25 mm (a). Experimental wavenumbers obtained with the plane wave test vector (dots) and the modified test vectors  $k^{\text{test}}(x)$  (circles) on wedged bone mimicking plates with central thickness  $e_0$  equal to 2.25 mm and  $\alpha$  equal to 1° (b) and (c) and 2° (d) and (e). Experimental wavenumbers are compared with the theoretical modes of the free plate of constant thickness  $e_0$  (continuous and dashed lines). Results of the propagation in the decreasing thickness direction (direction "–") are shown in (b) and (d). Results of the propagation in the increasing thickness direction (direction "+") are shown in (c) and (e). Thick arrows indicate portions of branches of guided mode not measured with any of the two methods. Thin arrows indicate portions of branches of guided modes measured only with the modified method. It corresponds to wavenumbers located in zone II of Fig. 4. The two examples shown in Figs. 3 an 4 are reported in (d) with the same symbols (large circle and star).

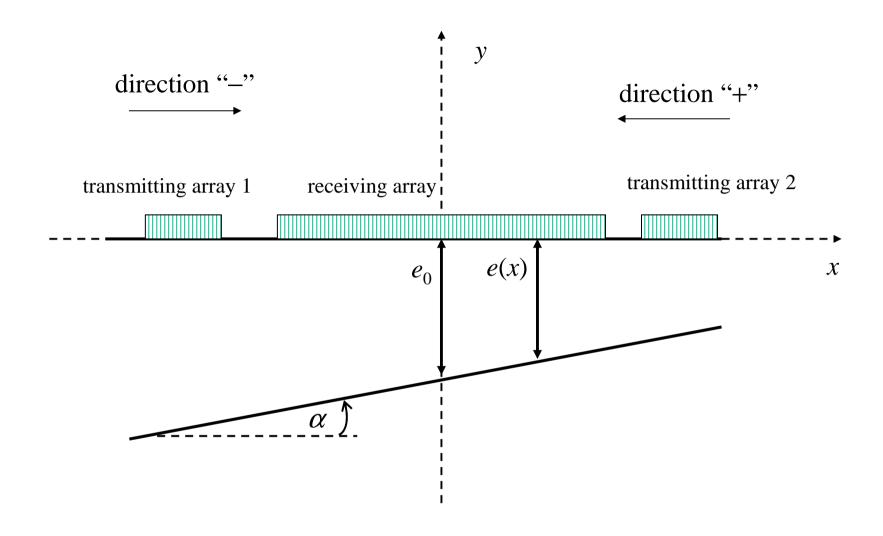
Figure 6. Theoretical (continuous and dashed lines) and experimental values of the deviation term  $\varepsilon(x_0, f)$  for  $\alpha = 1^\circ$  (a) and  $\alpha = 2^\circ$  (b), for modes A1 (circles), S2 (stars) and A3 (dots) for direction "—".

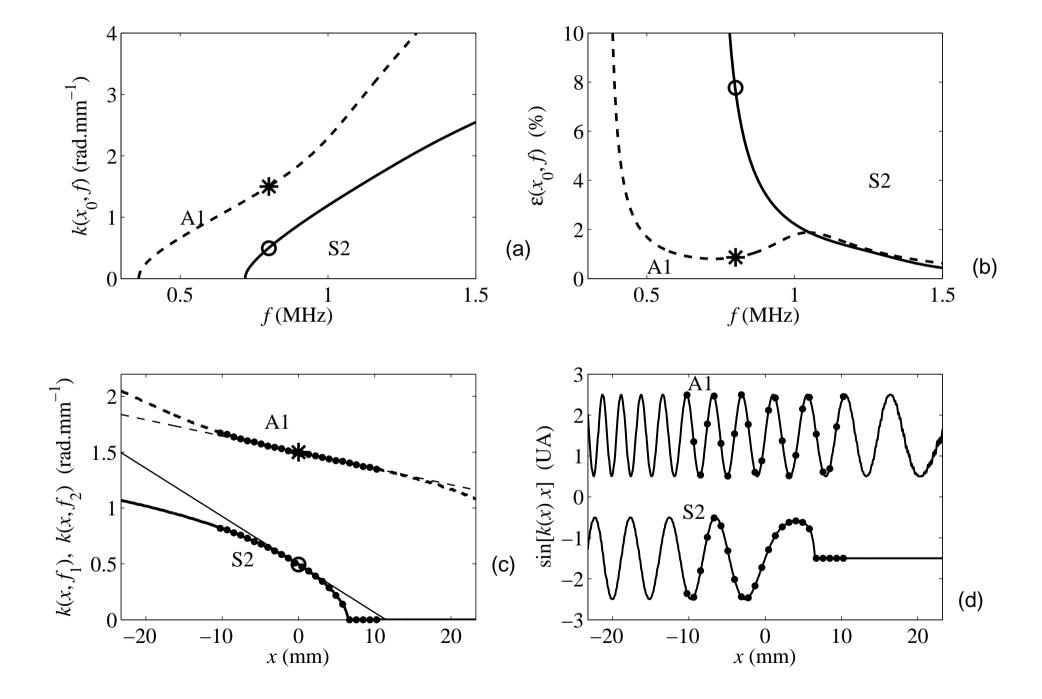


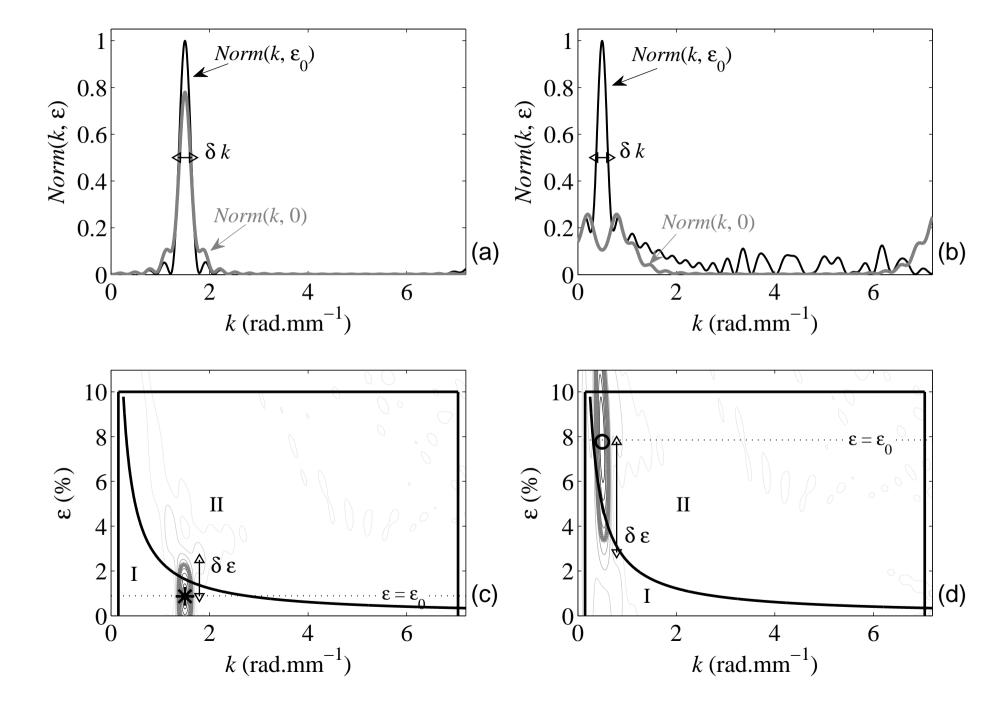


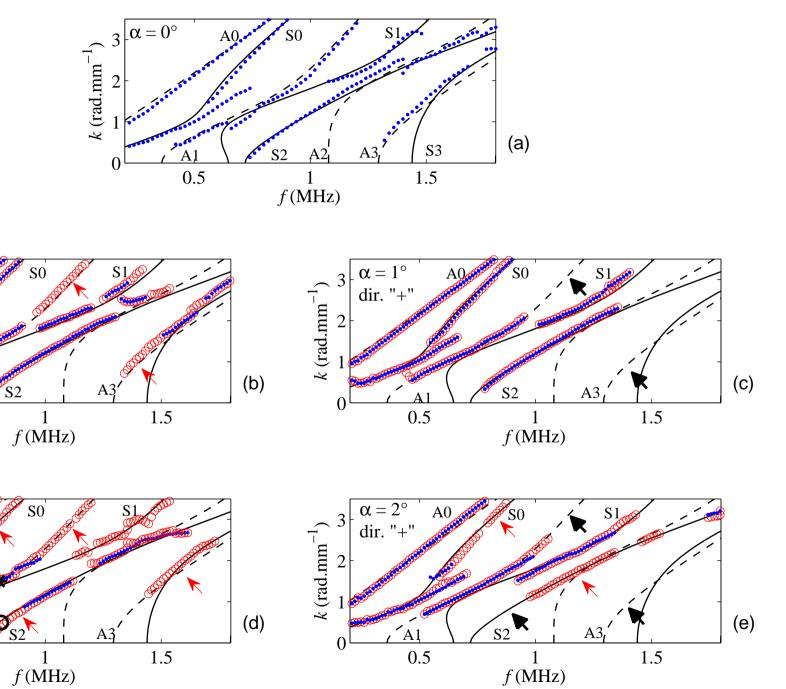












 $\alpha = 1^{\circ}$  dir. "-"

 $\frac{\alpha = 2^{\circ}}{\text{dir. "-"}}$ 

<u>A1</u> 0.5

A<sub>1</sub> 0.5

A0

 $k \text{ (rad.mm}^{-1})$ 

 $k (\text{rad.mm}^{-1})$ 

